Electrochimica Acta 457 (2023) 142429

Contents lists available at ScienceDirect

Electrochimica Acta

journal homepage: www.journals.elsevier.com/electrochimica-acta

Geneless optical control of cell redox balance in HL-1 cardiac muscle cells

Marco Malferrari [a,1,*], Gabriele Tullii [b,1], Carlotta Ronchi [b], Camilla Marzuoli [b,c], Ilaria Abdel Aziz [b], Maria Rosa Antognazza [b,*], Stefania Rapino [a,*]

[a] Dipartimento di Chimica "Giacomo Ciamician", Università di Bologna, via Francesco Selmi 2, Bologna 40126, Italy
[b] Center for Nano Science and Technology@PoliMi, Istituto Italiano di Tecnologia, via Rubattino 81, Milano 20134, Italy
[c] Dipartimento di Fisica, Politecnico di Milano, Piazza Leonardo da Vinci 32, Milano 20133, Italy

ARTICLE INFO

Keywords:
Redox balance
P3HT
Light
Scanning electrochemical microscopy
Cell proliferation
Reactive oxygen species
Conjugated polymers
Cell optical excitation

ABSTRACT

Photoactivation of conjugated polymers has been shown to be an attractive approach to modulate biological functions in several cell models; it is characterized by minimal invasiveness, high modulability, spatial selectivity at the level of single cells and even intracellular compartments. Reactive oxygen species produced by polymer photostimulation, in particular, were reported to trigger cell proliferation and recently proposed to finely modulate the cell cycle. Light-activated proliferation is extremely attractive for cardiac muscle cells, to overcome pathological conditions as heart failure and cardiovascular diseases with minimal invasiveness.

Here, we specifically address the target to optically modulate the cell redox balance of HL-1 cells, a cardiac muscle cell model, by localized photoexcitation of a light sensitive polymer, namely poly-3-hexyl-thiophene. Scanning electrochemical microscopy is employed to quantify the changes of the cellular redox balance. Both extracellular and intracellular production of reactive oxygen species upon illumination is investigated, by employing poly-3-hexyl-thiophene respectively in the form of thin films or nanoparticles. Our results show that light induced, spatially controlled production of reactive oxygen species by poly-3-hexyl-thiophene films in the extracellular compartment determines the shift of HL-1 redox balance towards more reducing values. Thus, highly resolved spatial control of the illuminated area enables modulation of HL-1 redox balance at the single cell level. The effect on cell redox balance of cytosol internalized poly-3-hexyl-thiophene nanoparticles is also presented.

Our work shows that photostimulation of conjugated polymers can be employed as a wireless, geneless technique to modulate on demand the intracellular redox balance, with high spatial resolution and minimal invasiveness, in a biologically relevant model of contractile, functioning cardiomyocytes. In perspective, this approach may be easily extended to other cell systems, wherever a fine control of the cell redox state is desirable, and open the path to innovative therapeutic tools.

1. Introduction

Cellular redox balance is a key parameter in cell physiology, governing the overall cell cycle (e.g. survival, differentiation, proliferation, up to specific function) [1,2]. The cell redox balance control is a highly pleiotropic phenomenon, influenced by positive, oxidative eustress as well as by detrimental, oxidative distress [3]. Under normal conditions, the intracellular concentration of reactive oxygen species (ROS) is in the nanomolar range (1–100 nM). Its delicate net balance results from the activity of numerous proteins and molecular processes within cells, which work either as ROS sources or ROS scavengers [1]. In such a narrow physiological concentration range, ROS mediate signaling through oxidation of proteins, mainly of the thiol groups of cysteine and tyrosine residues or of the metallic components of enzymes. As a matter of fact, all the cellular compartments are interested by ROS-mediated signaling; well-known transcription factors, such as NRF2 and NF-kB, have been reported to be controlled by ROS [3].

The importance of ROS in cell processes and their relevance as a therapeutic target prompted the development of several technical approaches, not only to quantify them in a physiologically relevant environment [4,5], but also to finely modulate their concentration. In fact, the possibility to trigger ROS production on demand, quantitatively,

* Corresponding authors.
E-mail addresses: marco.malferrari2@unibo.it (M. Malferrari), MariaRosa.Antognazza@iit.it (M.R. Antognazza), stefania.rapino3@unibo.it (S. Rapino).
[1] These authors contributed equally to this work.

https://doi.org/10.1016/j.electacta.2023.142429
Received 31 October 2022; Received in revised form 17 March 2023; Accepted 17 April 2023
Available online 18 April 2023

not-invasively, with a high spatial resolution (thus, targeting specific cell subpopulations or even cell organelles) is highly interesting both for the study of physiological state, and for the treatment of pathological conditions. Photo-activated ROS production, by means of low-light level phototherapy approach, has been proposed as a convenient strategy [6], considering the high selectivity and the high temporal and spatial resolution of light stimulation. The exploitation of cell endogenous, light-responsive, ROS producers, such as proteins (i.e. opsins or heme-proteins), has been also extensively investigated with interesting results [7,8]. However, the low absorbance of light-responsive proteins, as well as their variable expression in different tissues, reduce the efficiency and applicability of this approach. The possibility to employ exogenous, photo-electrochemically active materials is also currently investigated; in this approach precise and fine modulation of cellular processes is envisaged [6]. Among other possibilities, conjugated polymers are extremely convenient: they are excellent photo-transducers, and they are characterized by tunable optical properties, good photocatalytic efficiency, and optimal biocompatibility [9,10]. They have been employed in numerous biomedical applications involving stimulation of excitable cells, such as cortical and hippocampal neurons [11], retinal cells [12,13] and cardiomyocytes [14].

Poly-3-hexyl-thiophene (P3HT), a prototypical conjugated polymer, has been recently shown to foster the proliferation of cardiovascular cells; in particular, endothelial colony forming cells cultured on P3HT thin films and exposed to green light excitation displayed a strong enhancement of the tubulogenesis process [15,16]. It has been shown [17,18] that photostimulated P3HT thin films trigger Transient Receptor Potential Vanilloid 1 (TRPV1) opening, leading to calcium signaling modulation and to the activation of NF-ĸB transcription factor [15]. This observation has been unambiguously attributed to the occurrence of photoelectrochemical processes at the P3HT surface [19,20], leading to spatially localized production of ROS species, all virtually ending up in an increase of H_2O_2 concentration [21,22].

Cardiac muscle cells have been shown to be very sensitive to ROS and oxidative stress too: several developmental processes of cardiac muscle cells are regulated by ROS, and usually involve metabolic changes that lead to mitochondrial biogenesis able to sustain the developing heart. On another side, ROS and oxidative distress have been found to be involved in pathological conditions, for example in heart failure [23, 24]. One of the most serious factors in heart failure is the increase of ROS levels during reperfusion after an ischemic event [25], as a consequence of the myocardial ischemia, which could also lead to apoptosis of cardiomyocytes [2].

Photo-electrochemically active conjugated polymers thus represent a breakthrough strategy to precisely control intracellular ROS concentration. However, several questions remain currently open: (i) Is it possible to apply this technique to optically tune the cell redox balance, in a not-invasive manner? (ii) Is it possible to attain subcellular spatial resolution? (iii) Is it possible to use polymer nanoparticles (NPs), capable to cross the cell membrane, to effectively modulate the cell redox balance within the cell cytosol? (iv) Is it possible to modulate the redox balance in the specific case of cardiac muscle cells, in the perspective of a therapeutic application?

This work attempts to provide a first reply to the questions above. We use the prototypical P3HT conjugated polymer in the form of: (i) thin films, and we study how the spatially controlled, optical generation of ROS in the *extracellular space* influences the redox balance of HL-1 cells, a widely accepted murine cellular model of cardiac muscle cells [26]; (ii) nanoparticles internalized within the cell cytosol, and we explore an *intracellular mechanism* for ROS production. Consequently, we studied redox balance modulation driven by photo-generated ROS either outside or inside the cell membrane.

In this context, it is fundamental to assess whether an increase of ROS in the cytosol is produced, or an overall shift of cell redox midpoint potential to more reducing or oxidizing values takes place. Therefore, the main cell redox buffers, such as glutathione and NADH, must be taken into account. In the first case, local oxidative species could determine oxidation of biological components and promote the activation of redox signaling events (e.g. opening of protein channels, activation/deactivation of proteins) [27–29], while the overall shift of the cell redox balance might have different consequences on cellular physiology [2,30]. To quantify the cell redox balance and its modulation, we employ scanning electrochemical microscopy (SECM). SECM was successfully employed to investigate many biological processes in the last decades, both at the molecular and cellular levels [31–36]; in the last years, SECM underlined differences in cell redox balance between healthy and pathological human myocardium-derived mesenchymal stem cells [37,38]. Interestingly, a similar approach was used to study breast cells and to quantify, at the single-cell level, the cell redox balance in both healthy and tumor cells [39]. Very recently, SECM studies have been also preliminarily applied to P3HT interfaces in an aqueous environment, quantitatively confirming that spatially and temporally controlled production of ROS takes place upon illumination of P3HT films [21]. This process impacts on the redox state of cytochrome C, employed in that study as a model for redox proteins.

In this work, we directly address the possibility to optically modulate the cell redox balance, and we investigate the possibility to use prototypical P3HT conjugated polymer as a fully biocompatible extracellular or intracellular tool.

2. Experimental section

2.1. Preparation of ITO/P3HT substrates and P3HT NPs

P3HT thin film samples were fabricated by spin coating. Indium Tin Oxide (ITO)-coated glasses were used as substrates, and carefully cleaned, prior to deposition of polymer solution, by subsequent rinses in an ultrasonic bath (distilled water, acetone and isopropanol, 10 min each). Finally, they were dried with a nitrogen flux. rr-P3HT chlorobenzene solution (concentration, 20 $g \bullet L^{-1}$) was stirred at 50 °C for 15 h prior to spin coating deposition on ITO/glass substrates (1500 rpm, acceleration 1496 $rpm \bullet s^{-1}$).

P3HT NPs were prepared by employing the solvent diffusion method. A 1 mL solution of region-regular P3HT (purity, 99.995%; molecular weight, Mn 54.000–75.000; used as received from Sigma-Aldrich without further purification steps) 0.6 $g \bullet L^{-1}$ in tetrahydrofuran (Sigma Aldrich) was added dropwise to 10 mL of ultrapure water under magnetic stirring at 45 °C. The colloidal dispersion was sonicated for 20 min and treated with a rotary evaporator for 2 h for solvent removal. Finally, the P3HT NPs dispersion was subjected to dialysis against 2 L of water for 3 days, for complete removal of the residual organic solvent.

2.2. HL-1 cardiac muscle cell cultures and sample preparation

HL-1 murine cardiac muscle cells were purchased from MERCK (product number SCC065); cells were cultured in Claycomb medium (MERCK, product number 51800C) supplemented with 10% vol/vol North America Fetal Bovine Serum (MERCK product number 12103C), 0.1 mM norepinephrine, 2 mM L-glutamine, 100 $U \bullet ml^{-1}$ penicillin/streptomycin.

For the investigation of HL-1 cells adhering on P3HT/ITO and bare ITO substrates, we employed the following procedure for cell plating: Fibronectin (MERCK, product number F1141, 1 $mg \bullet ml^{-1}$) was deposited on P3HT/ITO and bare ITO substrates by overnight incubation at 37 °C in 2 $\mu g \bullet ml^{-1}$ fibronectin in Phosphate Buffered Saline (PBS) solution; after washing, $2 \bullet 10^4$ HL-1 $cells \bullet ml^{-1}$ were plated on 1 cm^2 squared substrates placed in Petri dishes (3.5 cm diameter) and placed at 5% CO_2 and 37 °C overnight in the incubator. Samples were measured at room temperature in Hank's Balanced Salt Solution (HBSS; MERCK, product number H8264) after washing with PBS.

P3HT nanoparticles uptake by HL-1 cells was performed as described in the following: HL-1 cells were plated on ITO substrates coated with 4

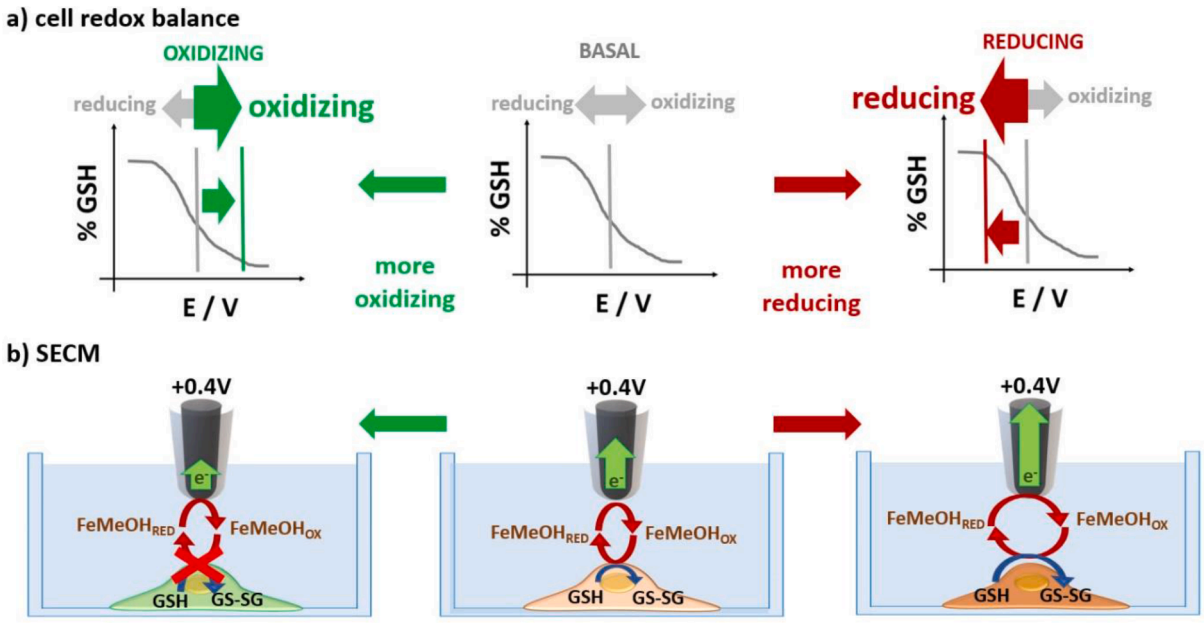

Fig. 1. Schematic representation of SECM imaging of cell redox balance with FeMeOH. In starting condition, at certain distance of the microelectrode with respect to the adhering cell (panel **b-BASAL**) a given oxidation current reports on the starting value of the cell redox balance (panel **a-BASAL**). A shift of the cell redox balance to a more oxidizing value (panel **a-OXIDIZING**) determines lower oxidation currents measured at the probe, as a consequence of lower cytoplasmic ratio of reduced glutathione (GSH/GS-SG) and lower regeneration of reduced FeMeOH (panel **b-OXIDIZING**). On the contrary, a shift of the cell redox balance to more reducing values reflects an increased ratio of GSH/GS-SG (panel **a-REDUCING**), higher regeneration of reduced FeMeOH and higher oxidation currents measured at the microelectrode (panel **b-REDUCING**). GSH, reduced glutathione; GS-SG, oxidized glutathione.

$\mu g \bullet ml^{-1}$ fibronectin solution for 3 h at 37 °C; after washing with PBS, HL1- cells were plated at $5 \bullet 10^4$ $cells \bullet ml^{-1}$. After adhesion, cells were incubated overnight with 10 $\mu g \bullet ml^{-1}$ P3HT nanoparticle suspension. The control samples were HL-1 cells adhering on ITO substrates not incubated with P3HT nanoparticle suspension. Samples were measured in HBSS medium at room temperature after washing with PBS solution.

2.3. Scanning electrochemical microscopy

SECM measurements were performed with CHI910B SECM from CH Instruments Inc. (Austin, Texas). A three electrodes setup was employed: an Ag/AgCl (3 M KCl) was used as reference electrode, a platinum wire as counter electrode and 10 μm platinum microelectrode as working electrode. Spatially controlled photostimulation of P3HT/ITO and bare ITO substrates was performed as described earlier [21]: excitation beam was obtained by focusing the light emitted from a mercury lamp of a Nikon Eclipse TiS inverted microscope filtered with a Nikon Texas Red HYQ cubic filter (excitation wavelength range, 532–587 nm; emission wavelength range, 608–683 nm). The power density measured at 550 nm was approximately 20 $mW \bullet mm^{-2}$.

HL-1 samples for SECM measurements were prepared for each type of experiment (i.e. HL-1 cells adhering on P3HT/ITO and bare ITO substrates, HL-1 incubated with P3HT nanoparticles) as detailed in paragraph 2.2. SECM imaging of cell redox balance and SECM approach curves were performed as described earlier [39] at room temperature in HBSS medium; 0.5 mM redox mediator, ferrocenemethanol or ferrocenecarboxilic acid, were dissolved in HBSS buffer and employed at this final concentration for both SECM images and approach curves. Before each experiment, HL-1 samples were washed with PBS and transferred to a 3.5 cm diameter Petri dish in 2.5 mL of 0.5 mM redox mediator (ferrocenemethanol or ferrocene carboxyl acid) in HBSS medium.

SECM images were performed by applying 0.4 V vs Ag/AgCl (KCl 3 M) to the working electrode and by employing a scanning speed of 25 $\mu m \bullet s^{-1}$; probe scan approach measurements were performed at 0.4 V vs Ag/AgCl (KCl 3 M), with 50% end current ratio. Probe scan approach measurements were analyzed with MIRA software [40]; insulator model [41] was shown to be inaccurate to fit all approach curves, while theoretical models considering a finite k constant [41] of charge exchange returned consistent results. Therefore, all approach curves were fitted using the latter model and the value of finite k constant took to quantify the shift of cell redox balance [39].

Black platinum-modified platinum microelectrodes, employed for ROS detection (Fig. S1), have been fabricated as described previously [21,32].

2.4. Intracellular ROS detection

2′,7′-dichlorodihydrofluorescein diacetate (H_2DCF–DA, purchased from Sigma Aldrich) was employed for intracellular detection of ROS. For the experiments with P3HT films, HL-1 cells were cultured on ITO and ITO/P3HT substrates (1.2×10^4 $cells \bullet cm^{-2}$). In the case of P3HT NPs, the cells were cultured on glass slides and half of the samples was incubated with P3HT NPs at 5 $\mu g \bullet mL^{-1} \bullet cm^{-2}$ concentration for 20 h. The remaining samples were not treated, as control condition (CTRL). The samples were rinsed with KRH to remove non-internalized NPs. The samples in light condition were photo-excited by illuminating each sample for 5 min with a LED system (Thorlabs, $\lambda = 530$ nm, 1.2 $mW \bullet mm^{-2}$). ITO/P3HT samples were illuminated from the ITO side. Subsequently, cells were incubated with H_2DCF–DA for 30 min (10 μM) in Krebs Ringer's (KRH) extracellular solution (mM): 135 NaCl, 5.4 KCl, 1.8 $CaCl_2$, 1 $MgCl_2$, 5 HEPES, 10 Glucose, pH adjusted to 7.4 with NaOH. After careful wash-out of the excess probe from the extracellular medium, the fluorescence of the probes was recorded (excitation/emission wavelengths, 490/520 nm; integration time, 500 ms; binning: 1×1) with an upright microscope (Olympus BX63) equipped with a 20X objective and a sCMOS Camera (Prime BSI, Teledyne Photometrics; Tucson, Arizona, USA). Variation of fluorescence intensity was evaluated over Regions of Interest covering single cell areas. Reported values represent the average over multiple cells ($n > 500$) belonging to 9 statistically independent samples, tested in 3 different experimental sessions. Image processing was carried out with ImageJ. Origin Pro 2018 was employed for data analysis.

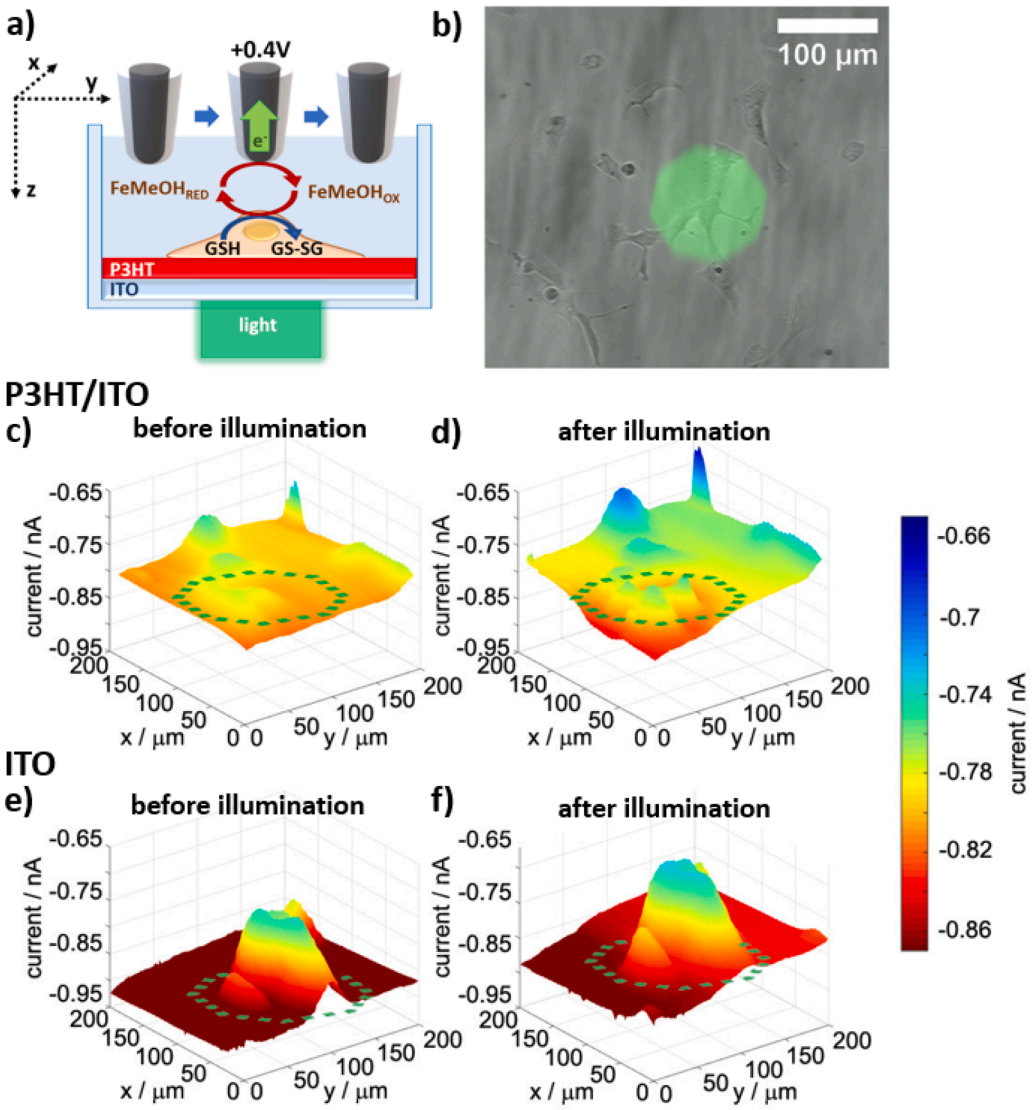

Fig. 2. (**a, b**) Experimental setup used for SECM measurements with spatially-controlled illumination of the sample. Schematic representation (**a**) of the measurement setup with a controlled illumination of HL-1 cells cultured on ITO/P3HT thin films. Cartesian axis references used in the manuscript is also reported. Oxidation of redox mediator at the microelectrode tip is schematically represented. Overlay of images (**b**) of the illumination spot (green) and phase contrast image of HL-1 cells plated on the top of ITO/P3HT substrates. **c-f**) SECM surfaces of cell redox balance of HL-1 cells plated on ITO/P3HT (**c, d**) or bare ITO (**e, f**) before and after illumination, respectively. Illumination area is located approximately between (x;y) coordinates in the (0–100; 0–100) range; localization of the area is represented by a dashed green octagon. SECM images were performed in the presence of 0.5 mM FeMeOH; illumination (λ = 532–587 nm) lasted for 1 min, see the Materials and Methods section for detailed description of the experimental conditions employed.

2.5. Confocal imaging

HL-1 cells were plated on glass slides at 1.2×10^4 cells•cm^{-2} density and were incubated with P3HT NPs at 5 µg mL^{-1}•cm^{-2} concentration for 20 h. Cell membrane and nuclei are stained, respectively, by Cell Mask Green (Thermo Fisher, exc/em wavelength, 522/535 nm) and HOECHST (Thermo Fisher, exc/em, 350/461 nm). Z-stacks were acquired with an upright microscope (Olympus BX63), equipped with a 60X water immersion objective, a spinning disk confocal module (X-Light V2 spinning disk module from Crest Optics), and a sCMOS Camera (Prime BSI, Teledyne Photometrics; Tucson, Arizona, USA). The system, comprising LED and laser light sources (Spectra III and Celesta, from Lumencor) was assembled by Crisel Instruments. Excitation/emission wavelengths were 530/660 nm for P3HT NPs. The experiments were carried out at room temperature and by employing KRH. Images were processed with ImageJ.

3. Results and discussion

SECM imaging of redox balance is based on the use of ferrocenemethanol (FeMeOH), as a membrane-permeable reporter of cell cytoplasmatic redox balance. To precisely quantify the cell redox balance, it is also important to have parallel information on the probe/cell distance during the imaging. Ferrocenecarboxilic acid (FeCOOH) is not able to permeate the cell membrane and is used to obtain SECM images reporting on the cell topography and allowing for a more precise estimation of the real cell/probe distance during the redox balance determination. Briefly, when the SECM ultramicroelectrode (UME) is set at 0.4 V versus Ag/AgCl (KCl 3 M), oxidation of FeMeOH takes place at the UME. When approached to the surface of cells, regeneration of the reduced form of FeMeOH from cell cytoplasm may be observed, as compared to the surfaces on which cells adhere; the regeneration of the pristine form of FeMeOH by the cells provokes an increase of the recorded currents (regeneration currents). The extent of this regeneration current is correlated to the cell redox balance: more the cell cytoplasmatic redox balance is shifted toward reducing values, higher the magnitude of the current increase will be (Fig. 1a,b). It has been shown that the ratio between reduced and oxidized glutathione (the more abundant redox buffering moiety in cell cytoplasm [2,30]) is the main determinant of the cytoplasmatic redox balance [39].

When FeCOOH, which is not permeable to the cell plasmatic membrane, is used, the oxidation currents recorded at the probe decrease as the probe approaches the cell. This is due to the well-known negative feedback regime: the cell (or any unreactive, insulating surface) hinders the diffusion of FeCOOH to the electrode causing a decrease of the recorded FeCOOH oxidation currents. Since the dependency of the

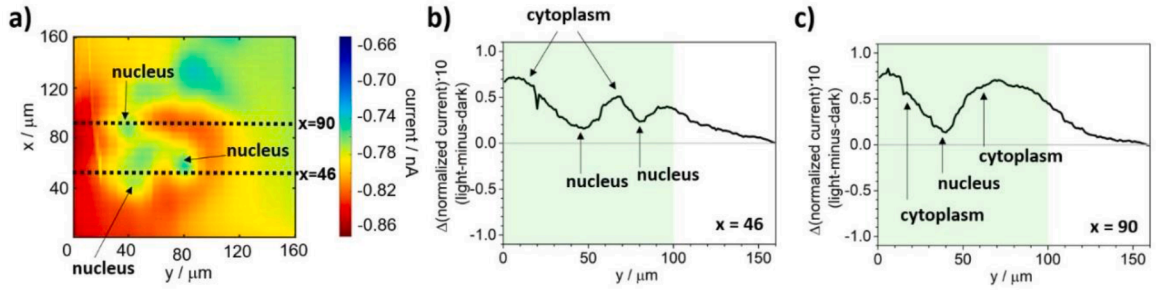

Fig. 3. Illumination effects on SECM images for HL-1 adhering on P3HT/ITO substrates. (**a**) SECM image of HL-1 cell redox balance after illumination; the x-sections considered in **b** and **c** panels are indicated by dashed lines. (**b,c**) Light-minus-dark differences of normalized oxidation currents: x-sections for $x = 46$ (**b**) and $x = 90$ (**c**) are showed. Illuminated regions are indicated by green transparent background.

decrease in the recorded currents on the probe/cell distances is well known, it is possible to obtain information on cell morphology (topography) from the recorded currents in presence of FeCOOH, when the probe is moved at constant height in the proximity of adhering cells or it is approached toward the cell from the top [31,39].

The cytoplasmatic cell redox balance was studied in presence of P3HT thin films spin casted on Indium Tin Oxide (ITO)-covered glasses (ITO/P3HT). Relevant to this study, previous SECM studies showed that spatially and temporally controlled production of ROS takes place upon illumination of P3HT films at the solid-liquid P3HT-water interfaces [21]. Hydrogen peroxide is produced at the solid-liquid P3HT-solution interface in a volume which is laterally defined by the boundaries of the illumination spot and within a distance of approximately 200 µm from the P3HT film surface. Interestingly, in that study cytochrome C was used as a model for redox proteins, in solution, and it was demonstrated that its redox state is deterministically affected by polymer photoexcitation.

Here, we make a pivotal step forward in the study of the interface, by carrying out SECM imaging of HL-1 cells seeded on top of ITO/P3HT substrates to evaluate the impact of polymer photoexcitation on the cell redox balance (Fig. 2a,b).

The experimental apparatus is schematized in Fig. 2a,b; HL-1 cells were plated at low density on the P3HT films coated by fibronectin (Fig. 2b; see the experimental section for detailed description of HL-1 culture and plating on substrates). As a control, SECM imaging was performed on HL-1 cells plated on ITO substrates coated with fibronectin only. Both images were acquired in Hank's Balanced Salt Solution (HBSS) medium in the presence of 0.5 mM FeMeOH. Light (excitation wavelength range 532–587 nm, light density 20 mW•mm^{-2}, overall duration 1 min) was focused within an octagonal area of approximately 12•10^3 µm^2 (Fig. 2b). This experimental condition enables the illumination of single or few HL-1 cells. Since SECM imaging was conducted to investigate cells in both illuminated and not illuminated regions, a direct comparison between optically excited and dark regions on the same sample is possible.

Fig. 2 reports SECM images of HL-1 cytoplasmatic redox balance for cells plated on ITO/P3HT (Fig. 2c and 2d, before and after illumination, respectively) or polymer-uncoated ITO (Fig. 2e and 2f, before and after illumination, respectively) substrates. We monitored the time course of hydrogen peroxide oxidation with black platinum-modified microelectrodes, positioned in the middle of the illuminated region at approximately 20 µm from the P3HT thin film (Fig. S1). A rapid disappearance

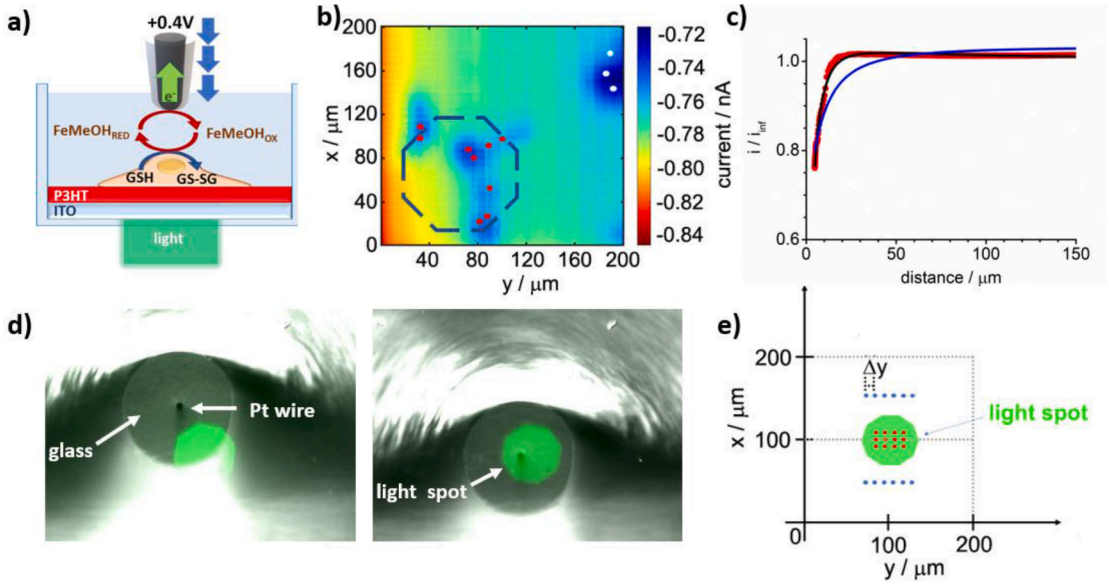

Fig. 4. SECM approach curve study of HL-1 cells adhering on ITO/P3HT substrates in the presence of 0.5 mM FeMeOH. (**a**) Schematic representation of SECM approaches on HL-1 cells adhering on ITO/P3HT substrates. (**b**) Example of approached points for illuminated cells (red) and not illuminated cells (white). The points are reported on the top of the SECM image recorded before SECM approach curves, as reference to precisely locate cells in the investigated space. (**c**) Example of SECM approach curve (red filled dots) and best fitting with an insulator (blue line) of finite k (black line) model. (**d**) Overlay of images of the approached platinum microelectrode corresponding to a position outside (left image) or inside (right image) of the illuminated portion of the P3HT films. (**e**) Scheme of the experimental design of investigation of ITO/P3HT substrate in absence of HL-1 cells. Red and blue dots represent sampling positions inside and outside the illuminated spot (green octagon in the scheme).

of ROS was demonstrated, as the oxidation signal goes back to the baseline levels in few seconds after switching off the light source. Consequently, the oxidation currents recorded in Fig. 2c–f are not due to hydrogen peroxide; the measurements are in fact accomplished at least 5 min after the illumination shut down, when as showed in Fig. S1 hydrogen peroxide concentration is negligible in the vicinity of P3HT surface or diffused away in the bulk. Fig. 2d clearly shows an increase of oxidation currents in HL-1 cells following illumination, while no relevant differences could be documented neither for not illuminated cells adhering onto ITO/P3HT (Fig. 2c), nor for illuminated cells plated onto bare ITO (Fig. 2f). The increase of oxidation current reports for a shift of the redox balance towards more reducing conditions (*vide* Fig. 1a,b).

Fig. 3 shows representative SECM section images at specific x coordinates ($x = 46$ μm, $x = 90$ μm; Fig. 3a). Interestingly, the increase of oxidation current is predominantly located at the cell periphery/cytosol of HL-1 cells exposed to optical excitation, while it is less relevant at the nuclear regions (Fig. 3b and 3c). No relevant increase of oxidation current could be imaged when illuminated ITO/P3HT substrates in the absence of cells were investigated (see Fig. S2). These results support the hypothesis that hydrogen peroxide, produced at the solid-liquid interface upon polymer optical excitation, diffuses into (or indirectly affects) cell cytoplasm and produces a shift of the inner cell redox balance towards more reducing values.

This behavior is consistent with what previously observed in tumor breast cancer cell lines [39]: in fact, investigations on tumor breast cancer cells clearly put in evidence that by adapting to a more oxidative metabolism, typical of cancer cells, a shift to more reducing values of cell redox balance is observed as compared to healthy cells. SECM imaging of HL-1 cells adhering on ITO/P3HT substrates was performed also in the presence of FeCOOH as redox mediator, to evaluate whether illumination provokes changes in cell morphology: the results show that no relevant differences can be observed between illuminated and not illuminated cells (Fig. S3).

To quantify the shift of the redox balance, we performed a detailed study of SECM approach curves on both illuminated and not illuminated HL-1 cells plated on ITO/P3HT substrates (Fig. 4). The scheme of the set up and of the type of measurements performed is shown in Fig. 4a: cells are approached with the microelectrode along the z direction, from the bulk of the buffer solution towards the Petri dish surface. Fig. 4b reports a representative example of approached points for illuminated cells (red, within the light spot octagonal area) and not illuminated cells (white, outside the light spot). This technique has been already employed for the characterization of numerous surface properties and provides, if coupled to a solid theoretical derivation, valuable information about the reactivity of the analyzed sample [31,34,41,36,42–44]. Several investigations were performed on single isolated cells, and a detailed description of the permeation of both hydrophilic and hydrophobic redox mediators through plasmatic membrane of adhering cells was provided [5,45,46]. When an insulating surface is approached, negative feedback curves are obtained, due to the hindering of the diffusion of the redox mediator to the active tip of the microelectrode provoked by the surface. In our measurements (an example of a SECM approach curve is showed in Fig. 4c), the approached cell cytoplasm can partially regenerate the reduced form of FeMeOH and an increase of the measured oxidation current at the microelectrode tip is observed. As aforementioned, FeMeOH/ $FeMeOH^+$ freely diffuses across the cell plasmatic membrane and can interact with the inner cell redox species: more reducing is the inner cell redox environment, higher will be the current increase (higher regenerative current will be measured). In this case, a finite kinetics behavior characterizes the approach curves. More precisely, best fitting of SECM approach curves return values of the heterogeneous charge transfer kinetic constant, k, which is directly correlated to the capability of the cell cytoplasm to regenerate FeMeOH in the reduced/pristine form; higher the kinetic constant, more reducing is the inner cell redox environment.

Interestingly, SECM approach curves (both before and after illumination) cannot be accurately fitted by a pure insulator model (blue line in Fig. 4c); a fully satisfactory fitting is instead obtained when a finite k constant is considered (black line in Fig. 4c) [41].

Table 1
Values of finite k constant and t-test results (two tails analysis, heterogeneous variance) for SECM approach curve analysis; n.s., not significantly different; $p < 0.05$, significantly different; n, number of SECM approach curves.

	n	Finite k values		p values
		Before light	After light	
HL-1 cells plated on ITO/P3HT substrates				
Illuminated cells	9	0.14 ± 0.03	0.18 ± 0.04	**$p < 0.05$**
Not illuminated cells	6	0.12 ± 0.03	0.12 ± 0.04	n.s.
HL-1 cells plated on ITO substrates				
Illuminated cells	13	0.10 ± 0.03	0.07 ± 0.01	n.s.
Not illuminated cells	9	0.12 ± 0.05	0.09 ± 0.03	n.s.
ITO/P3HT substrates in the absence of HL-1 cells				
Illuminated P3HT	12	0.12 ± 0.02	0.13 ± 0.02	n.s.
Not illuminated P3HT	12	0.10 ± 0.03	0.09 ± 0.03	n.s.

The results of the SECM approach analyses are reported in Table 1: when charge transfer constant values k before and after illumination are compared, a significant k increase was documented only for illuminated cells grown on top of ITO/P3HT substrates. Conversely, no relevant differences were obtained neither for not illuminated cells, nor for control, i.e. HL-1 cells adhering on bare ITO substrates (Table 1). To demonstrate that the increase of the oxidation current is not due to changes in the conductivity of the P3HT films, the same study was also carried out on ITO/P3HT substrates in the absence of cells. Representative images obtained with an inverted fluorescence microscope are reported in Fig. 4d, showing the scanning microelectrode position outside and inside the illuminated area (left and right, respectively). The scheme of the experiment is represented in Fig. 4e; the k values obtained by the fitting of the approach curves are reported in Table 1.

Fig. 5a shows a plot of the finite charge transfer constant values k, after- versus before- illumination for ITO/P3HT substrate, both in the presence of adhering HL-1 cells and in their absence. This representation returns a summary of the results and shows the dispersion of the experimental points. Should no changes occur upon illumination, all experimental points will align on the median line. The average dispersion of the experimental points around the median line in the plot reports on the heterogeneity of the biological samples; this graph highlights the significant increase in the finite charge transfer constant k values, which is observed when HL-1 cells are grown on P3HT.

Overall, this result quantitatively demonstrates that, upon photostimulation, HL-1 cells grown on ITO/P3HT substrate show a shift toward more reducing values of the cell redox balance, caused by the extra-cytoplasmic hydrogen peroxide locally produced by illumination of the polymer film. This effect could be reasonably attributed to the interaction between cells and ROS photoproduced by the polymer film in the extracellular matrix. However, at this stage it is not possible to discriminate whether the redox balance change is caused directly by ROS species diffusing into the cytoplasm or the effect is instead mediated by processes fostered by the presence of ROS species in the extracellular environment. To elucidate this point, we investigated the redox balance by SECM approach curves of HL-1 cells incubated with P3HT NPs. The latter usually cross the cell membrane, as previously proven in several cell line models, and maintain their photocatalytic properties while being inside the cell cytoplasm, thus generating ROS inside the cells upon photoexcitation. In this case, HL-1 cells were incubated overnight with P3HT NPs (see the experimental section for more details). The results are reported in Fig. 5b: it appears that just following incubation with P3HT NPs, independently on illumination, a relevant and systematic increase of the charge transfer finite k constant values of the cells is observed. This observation is consistent with a shift of the inner cell redox balance toward more reducing potential caused by the mere presence of the NPs. However, in this case no further changes of redox

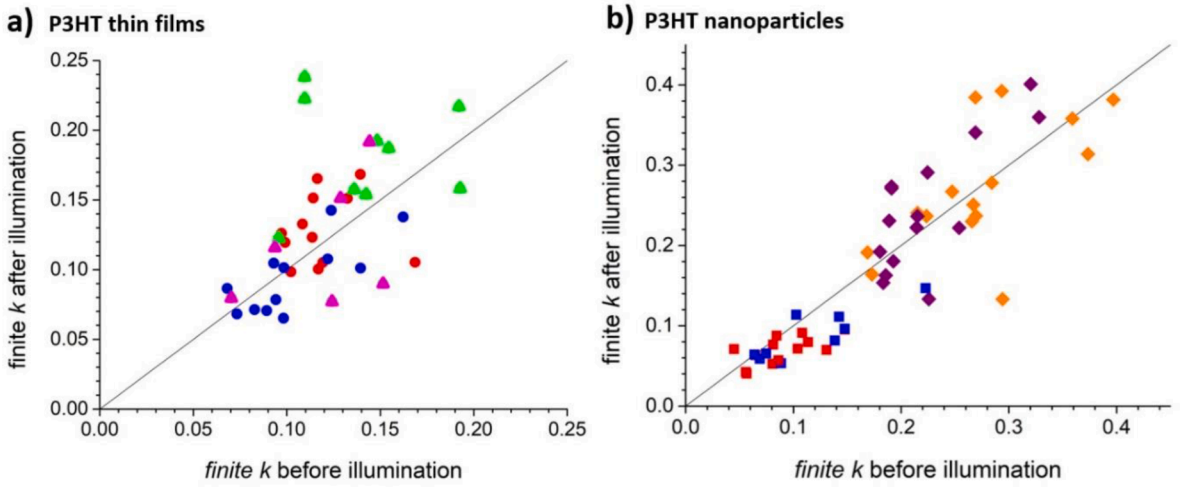

Fig. 5. Finite charge transfer constant *k* after illumination versus finite *k* constant before illumination. (**a**) HL-1 cells grown on P3HT/ITO substrate and the substrate itself. Filled dots represent *k* values obtained for ITO/P3HT substrates without cells, for illuminated (red) and not illuminated (blue) area; filled triangles represent *k* values measured for illuminated (green) and not illuminated (magenta) HL-1 cells adhering on ITO/P3HT substrates. (**b**) Investigations conducted in the presence of adhering HL-1 cells incubated or not with P3HT NPs. Filled squares represent *k* values obtained for HL-1 cells not incubated with NPs before (blue) and after (red) illumination, while filled rhombuses *k* values measured for HL-1 cells incubated with P3HT NPs before (purple) or after (orange) illumination.

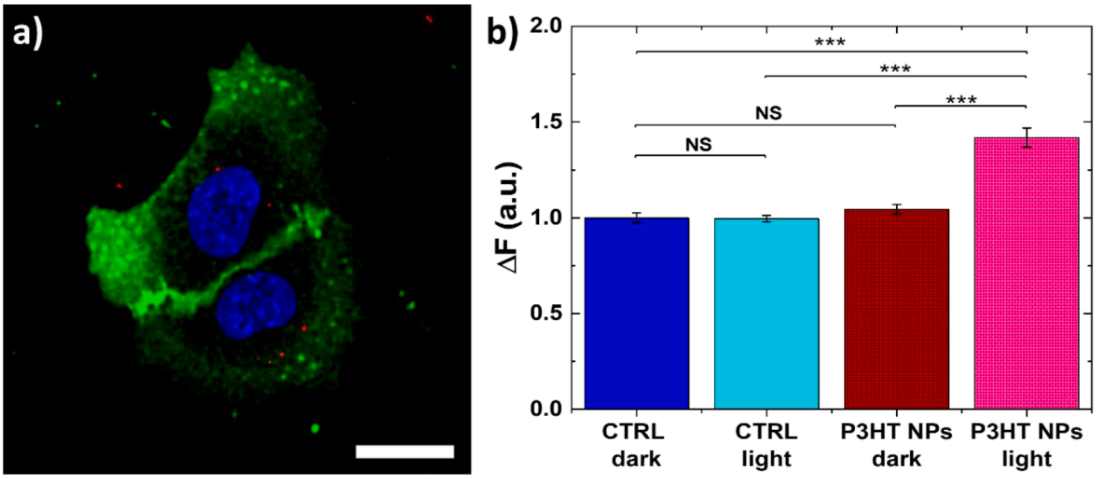

Fig. 6. (**a**) Representative confocal image depicting HL-1 cells loaded with P3HT NPs acquired at a z plane corresponding to the cell inner part. Cells are stained with Cell mask green (membrane, green) and Hoechst 33,342 (nuclei, blue). NPs intrinsic emission is in red. Scale bar, 10 μm. (**b**) Fluorescence intensity (ΔF) of the ROS-sensitive DCF probe internalized within HL-1 cells treated/untreated with P3HT NPs, in light and dark conditions. DCF probe excitation/emission wavelengths: 488/515 nm. Error bars represent the standard error of the mean (sem), ***p < 0.001 (Student's *t*-test).

balance of HL-1 cells, treated with P3HT NPs, are observed upon illumination. This behavior may be ascribed to the different redox balance of the cells when exposed to NPs.

These latter results highlighted the need for (i) verifying P3HT NPs effective internalization in HL-1 cells (ii) comparing the amount of ROS detectable in HL-1 cytoplasm following illumination for P3HT/ITO thin films and P3HT NPs.

First, we investigated the capability of NPs to efficiently internalize within the HL-1 intracellular environment, by means of confocal microscopy (Figs. 6a and S4). Confocal images are acquired at different z planes from the cell upper surface to the bottom interface (Fig. S4). Images recorded at a focal plane corresponding to the cell half height, in the middle of the cell volume, clearly show that P3HT NPs (red) are successfully internalized within the cellular membrane (green), without however crossing the nuclear membrane (blue, Fig. 6a), in agreement with previous observations in other cell models.

The intracellular ROS production was measured, both in dark and upon photoexcitation, by means of 2,7-dichlorodihydrofluorescein diacetate (H_2DCF–DA) fluorescent probe, which is sensitive to a large variety of different ROS, including H_2O_2, $HO^{\cdot}$, $ROO^{\cdot}$. H_2DCF-DA is intrinsically non-fluorescent; when it is internalized within the cell cytosol, it is firstly hydrolyzed by cellular esterase and the subsequent oxidation by ROS leads to the fluorescent compound 2,7-dichlorofluorescein (DCF). Fig. 6b depicts the DCF fluorescence intensity (ΔF) recorded in HL-1 cells with and without P3HT NPs, both in dark and upon green light excitation (λ=530 nm, 5 min, 1.2 mW/mm^2). The results highlight that the illumination of P3HT NPs within the cell cytoplasm induces a significant increase in the ROS intracellular concentration, as compared to the control samples, in agreement with previous results obtained with HEK 293T cells [7].

The experiment was repeated in the case of HL-1 cells grown on top of bare ITO and ITO/P3HT substrates. Similarly to what already observed with ECFCs [18], a relative fluorescence difference (i.e., intracellular ROS concentration) is obtained in the case of the cells grown on top of P3HT and subjected to light excitation, with respect to control conditions, i.e. non-illuminated cells, or cells plated on bare ITO

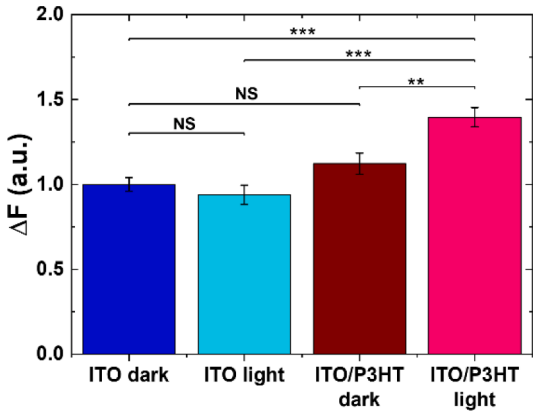

Fig. 7. Fluorescence intensity (ΔF) of the ROS-sensitive DCF probe internalized within HL-1 cells plated on ITO and ITO/P3HT substrates, in light and dark conditions. DCF probe excitation/emission wavelengths: 488/515 nm. Data were compared using the nonparametric Mann-Whitney U-test (0.05 significance level). ** $p < 0.01$, *** $p < 0.001$. Error bars represent the standard error of the mean (sem).

upon photoexcitation (Fig. 7). This result points out that the change in the inner redox balance observed in HL-1 cells, extracellularly stimulated by photoexcited P3HT films, is accompanied by an increase in the cytosolic ROS concentration.

Results obtained in the case of P3HT/ITO thin films and P3HT NPs are summarized in Fig. 8. In brief, in the dark the HL-1 redox balance does not show significant changes in the case of P3HT/ITO samples (Fig. 8, a1 and a2), while it shifts to more reducing values in the case of P3HT NPS (Fig. 8, b1 and b2). Upon photoexcitation of P3HT thin film, ROS are generated in the extracellular space, turning into reduced HL-1 redox balance (Fig. 8, a3 and a4). P3HT NPs illumination, instead, does not lead to additional reducing effect as compared to NPs-treated HL-1 in dark (Fig. 8, b3 and b4).

Overall, these results point out that the two forms of the conjugated polymer, while both leading to an increase in the intracellular ROS concentration upon light, have a different effect on the cell redox balance and state. We can interpret these findings as due to: (i) the different location of ROS production. Thin films and NPs photoexcitation both lead to cytosol ROS concentration increase, but only in the first case the local activation of membrane channels is expected to play a role in the change in the cell redox balance; (ii) different amounts of ROS could be produced in the two situations. The oxidative species that are produced upon illumination of P3HT NPs (as showed in Fig. 6b) might initiate redox signaling and trigger cell physiological phenomena (e.g. proliferation) already documented in the literature [15–18], without however appreciably altering the overall cell redox balance. Interestingly, the NP internalization by itself provokes a shift of the cell redox balance toward more reducing values in dark conditions (Fig. 5b). A putative explanation may be that the higher buffering capacity (toward the ROS produced) of the cell redox environment, when P3HT NPs are internalized, may lead to a different fate of the produced ROS, activating different signaling processes and pathways. In addition, the different location of ROS production, i.e. extracellular vs. intracellular, may result in a substantially different response of the cell to the ROS stimuli. However,

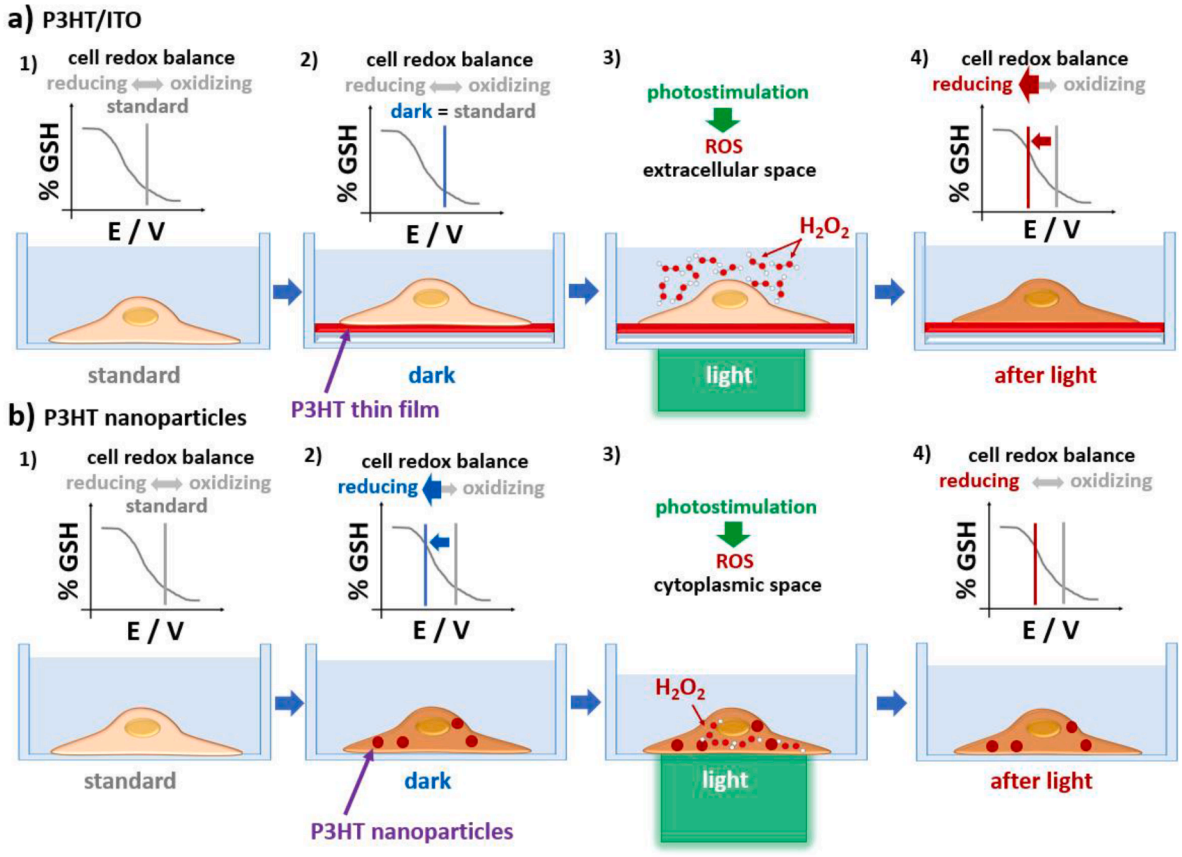

Fig. 8. Summary of cell redox balance changes of HL-1 cardiac cells following photostimulation of P3HT/ITO films and P3HT nanoparticles. (**a**) HL-1 cells adhering on P3HT/ITO substrates: in the dark redox balance (schematically represented in the upper graphs) does not change significantly for cells adhering on the substrate as compared to control (**a2** as compared to **a1**). Following photoinduced production of ROS in the extracellular space by P3HT/ITO substrates (**a3**) HL-1 redox balance shifts to more reducing value (**a4**). (**b**) P3HT nanoparticles internalization by HL-1 (**b2**) in the dark shifts HL-1 redox balance to more reducing values; ROS production in HL-1 cytoplasm following P3HT nanoparticles illumination (**b3**) does not further shifts HL-1 redox balance (**b4**).

further investigations are needed to check this hypothesis, and will be the object of a future work.

4. Conclusions

In the present work we investigated the effect of spatially and controlled ROS production on redox balance of a cardiac muscle cell model; extracellular or intracellular ROS increase was obtained by photostimulation of P3HT films and P3HT nanoparticles, respectively.

Increase of ROS concentration in the extracellular space of HL-1 cells adhering on P3HT/ITO substrates provoked the shift of HL-1 redox balance toward more reducing values, while no effect was documented in the dark. However, the mere internalization of P3HT nanoparticles in the dark was shown to produce a shift of HL-1 redox balance toward more reducing values; no further relevant change of the cell redox balance was documented upon photostimulation. Regarding ROS production in cell cytoplasm upon illumination, an increase of oxidative species for both light-activated P3HT films and nanoparticles was documented.

These results proved that it is possible to optically modulate cardiac muscle cell redox balance by P3HT excitation. In the case of P3HT films, extracellular ROS production enables to shift it, on demand, to more reducing values. Results obtained for P3HT nanoparticles highlighted that modulation of cell redox balance is independent on optical stimulation. This interesting effect deserves an in depth, dedicated study, for instance by employing nanoparticles with different physical-chemical properties (e.g., different Z potentials, surfactants, dimensions, surface properties, internalization capability), thus allowing one to elucidate what are the main drivers of the shift of HL-1 redox balance in the absence of optical stimulation.

Author contributions

M.M. and G.T. contributed equally. M.M. performed the SECM experiments. G.T. and I.A.A. prepared polymer thin films. G.T. prepared polymer NPs. C.M. and G.T. carried out confocal imaging and fluorescence ROS measurements. C.R. prepared HL-1 cell cultures. All authors discussed the data. M.M. and S.R. drafted the manuscript, and all the authors contributed to the writing of the manuscript. M.M., M.R.A. and S.R. designed the research. M.R.A. and S.R. supervised the research. All authors have given approval to the final version of the manuscript.

Declaration of Competing Interest

The authors report no conflict of interest.

Data availability

Data will be made available on request.

Acknowledgements

This research was supported by: EU Horizon 2020 FETOPEN-2018-2020 Programme 'LION-HEARTED', grant agreement n. 828984 (MM, CM, CR, MRA, SR); European Research Council (ERC) under the European Union's Horizon 2020 research and innovation program 'LINCE', grant agreement n. 803621 (GT, IAA, MRA).

Supplementary materials

Supplementary material associated with this article can be found, in the online version, at doi:10.1016/j.electacta.2023.142429.

References

[1] S. Parvez, M.J.C. Long, J.R. Poganik, Y. Aye, Redox signaling by reactive electrophiles and oxidants, Chem. Rev. 118 (2018) 8798–8888, https://doi.org/10.1021/acs.chemrev.7b00698.
[2] H. Sies, D.P. Jones, Reactive oxygen species (ROS) as pleiotropic physiological signalling agents, Nat. Rev. Mol. Cell Biol. 21 (2020) 363–383, https://doi.org/10.1038/s41580-020-0230-3.
[3] H. Sies, Role of metabolic H2O2 generation: redox signaling and oxidative stress, J. Biol. Chem. 289 (2014) 8735–8741, https://doi.org/10.1074/jbc.R113.544635.
[4] S.I. Dikalov, R.R. Nazarewicz, Measurements of reactive oxygen species in cardiovascular studies, Syst. Biol. Free Radic. Antioxid. (2012) 1437–1450, https://doi.org/10.1007/978-3-642-30018-9_45.
[5] M. Malferrari, M. Becconi, S. Rapino, Electrochemical monitoring of reactive oxygen/nitrogen species and redox balance in living cells, Anal. Bioanal. Chem. 411 (2019) 4365–4374, https://doi.org/10.1007/s00216-019-01734-0.
[6] M.R. Antognazza, I.A. Aziz, F. Lodola, Use of exogenous and endogenous photomediators as efficient ROS modulation tools: results and perspectives for therapeutic purposes, Oxid. Med. Cell. Longev. 2019 (2019), https://doi.org/10.1155/2019/2867516.
[7] C. Bossio, I. Abdel Aziz, G. Tullii, E. Zucchetti, D. Debellis, M. Zangoli, F. Di Maria, G. Lanzani, M.R. Antognazza, Photocatalytic activity of polymer nanoparticles modulates intracellular calcium dynamics and reactive oxygen species in HEK-293 cells, Front. Bioeng. Biotechnol. 6 (2018) 1–17, https://doi.org/10.3389/fbioe.2018.00114.
[8] L.F. De Freitas, M.R. Hamblin, Proposed mechanisms of photobiomodulation or low-level light therapy, IEEE J. Sel. Top. Quantum Electron. 22 (2016) 348–364, https://doi.org/10.1109/JSTQE.2016.2561201.
[9] E. Marin, N. Tiwari, M. Calderón, J.R. Sarasua, A. Larrañaga, Smart layer-by-layer polymeric microreactors: PH-Triggered drug release and attenuation of cellular oxidative stress as prospective combination therapy, ACS Appl. Mater. Interfaces 13 (2021) 18511–18524, https://doi.org/10.1021/acsami.1c01450.
[10] H. Palza, P.A. Zapata, C. Angulo-Pineda, Electroactive smart polymers for biomedical applications, Materials (Basel) 12 (2019), https://doi.org/10.3390/ma12020277.
[11] D. Ghezzi, M.R. Antognazza, M. Dal Maschio, E. Lanzarini, F. Benfenati, G. Lanzani, A hybrid bioorganic interface for neuronal photoactivation, Nat. Commun. 2 (2011), https://doi.org/10.1038/ncomms1164.
[12] D. Ghezzi, M.R. Antognazza, R. MacCarone, S. Bellani, E. Lanzarini, N. Martino, M. Mete, G. Pertile, S. Bisti, G. Lanzani, F. Benfenati, A polymer optoelectronic interface restores light sensitivity in blind rat retinas, Nat. Photonics 7 (2013) 400–406, https://doi.org/10.1038/nphoton.2013.34.
[13] V. Gautam, D. Rand, Y. Hanein, K.S. Narayan, A polymer optoelectronic interface provides visual cues to a blind retina, Adv. Mater. 26 (2014) 1751–1756, https://doi.org/10.1002/adma.201304368.
[14] F. Lodola, V. Vurro, S. Crasto, E. Di Pasquale, G. Lanzani, Optical pacing of human-induced pluripotent stem cell-derived cardiomyocytes mediated by a conjugated polymer interface, Adv. Healthc. Mater. 8 (2019) 1–7, https://doi.org/10.1002/adhm.201900198.
[15] F. Lodola, V. Rosti, G. Tullii, A. Desii, L. Tapella, P. Catarsi, D. Lim, F. Moccia, M. R. Antognazza, Conjugated polymers optically regulate the fate of endothelial colony-forming cells, Sci. Adv. 5 (2019) 1–13, https://doi.org/10.1126/sciadv.aav4620.
[16] F. Moccia, M.R. Antognazza, F. Lodola, Towards novel geneless approaches for therapeutic angiogenesis, Front. Physiol. 11 (2021), https://doi.org/10.3389/fphys.2020.616189.
[17] S. Negri, P. Faris, V. Rosti, M.R. Antognazza, F. Lodola, F. Moccia, Endothelial TRPV1 as an emerging molecular target to promote therapeutic angiogenesis, Cells 9 (2020) 1–29, https://doi.org/10.3390/cells9061341.
[18] S. Negri, P. Faris, G. Tullii, M. Vismara, A.F. Pellegata, F. Lodola, G. Guidetti, V. Rosti, M.R. Antognazza, F. Moccia, Conjugated polymers mediate intracellular Ca^{2+} signals in circulating endothelial colony forming cells through the reactive oxygen species-dependent activation of Transient Receptor Potential Vanilloid 1 (TRPV1), Cell Calcium 101 (2022), 102502, https://doi.org/10.1016/j.ceca.2021.102502.
[19] E. Zeglio, O. Inganäs, Active materials for organic electrochemical transistors, Adv. Mater. 30 (2018), https://doi.org/10.1002/adma.201800941.
[20] G. Milczarek, O. Inganäs, Renewable cathode materials from biopolymer/conjugated polymer interpenetrating networks, 335 (2012) 1468–1472. 10.1126/science.1215159.
[21] I. Abdel Aziz, M. Malferrari, F. Roggiani, G. Tullii, S. Rapino, M.R. Antognazza, Light-triggered electron transfer between a conjugated polymer and cytochrome c for optical modulation of redox signaling, iScience 23 (2020), 101091, https://doi.org/10.1016/j.isci.2020.101091.
[22] O.S. Abdullaeva, I. Sahalianov, M. Silverå Ejneby, M. Jakešová, I. Zozoulenko, S. I. Liin, E.D. Głowacki, Faradaic pixels for precise hydrogen peroxide delivery to control M-type voltage-gated potassium channels, Adv. Sci. 9 (2022) 1–14, https://doi.org/10.1002/advs.202103132.
[23] J.L. Pohjoismäki, S. Goffart, The role of mitochondria in cardiac development and protection, Free Radic. Biol. Med. 106 (2017) 345–354, https://doi.org/10.1016/j.freeradbiomed.2017.02.032.
[24] M. Bonora, C. Giorgi, P. Pinton, Molecular mechanisms and consequences of mitochondrial permeability transition, Nat. Rev. Mol. Cell Biol. (2021), 0123456789, https://doi.org/10.1038/s41580-021-00433-y.

[25] S. Cadenas, ROS and redox signaling in myocardial ischemia-reperfusion injury and cardioprotection, Free Radic. Biol. Med. 117 (2018) 76–89, https://doi.org/10.1016/j.freeradbiomed.2018.01.024.
[26] W.C. Claycomb, N.A. Lanson, B.S. Stallworth, D.B. Egeland, J.B. Delcarpio, A. Bahinski, N.J. Izzo, HL-1 cells: a cardiac muscle cell line that contracts and retains phenotypic characteristics of the adult cardiomyocyte, Proc. Natl. Acad. Sci. USA 95 (1998) 2979–2984, https://doi.org/10.1073/pnas.95.6.2979.
[27] B. D'Autréaux, M.B. Toledano, ROS as signalling molecules: mechanisms that generate specificity in ROS homeostasis, Nat. Rev. Mol. Cell Biol. 8 (2007) 813–824, https://doi.org/10.1038/nrm2256.
[28] M. Malferrari, P. Turina, F. Francia, A. Mezzetti, W. Leibl, G. Venturoli, Dehydration affects the electronic structure of the primary electron donor in bacterial photosynthetic reaction centers: evidence from visible-NIR and light-induced difference FTIR spectroscopy, Photochem. Photobiol. Sci. 14 (2015) 238–251, https://doi.org/10.1039/c4pp00245h.
[29] L. Diebold, N.S. Chandel, Mitochondrial ROS regulation of proliferating cells, Free Radic. Biol. Med. 100 (2016) 86–93, https://doi.org/10.1016/j.freeradbiomed.2016.04.198.
[30] D.P. Jones, H. Sies, The redox code, Antioxid. Redox Signal. 23 (2015) 734–746, https://doi.org/10.1089/ars.2015.6247.
[31] L. Bartolini, M. Malferrari, F. Lugli, F. Zerbetto, F. Paolucci, P.G. Pelicci, C. Albonetti, S. Rapino, Interaction of single cells with 2D organic monolayers: a scanning electrochemical microscopy study, ChemElectroChem. 5 (2018) 2975–2981, https://doi.org/10.1002/celc.201800731.
[32] M. Malferrari, A. Ghelli, F. Roggiani, G. Valenti, F. Paolucci, M. Rugolo, S. Rapino, Reactive oxygen species produced by mutated mitochondrial respiratory chains of entire cells monitored using modified microelectrodes, ChemElectroChem 6 (2019) 627–633, https://doi.org/10.1002/celc.201801424.
[33] R. Borghese, M. Malferrari, M. Brucale, L. Ortolani, M. Franchini, S. Rapino, F. Borsetti, D. Zannoni, Structural and electrochemical characterization of lawsone-dependent production of tellurium-metal nanoprecipitates by photosynthetic cells of Rhodobacter capsulatus, Bioelectrochemistry 133 (2020), 107456, https://doi.org/10.1016/j.bioelechem.2020.107456.
[34] T.E. Lin, S. Rapino, H.H. Girault, A. Lesch, Electrochemical imaging of cells and tissues, Chem. Sci. 9 (2018) 4546–4554, https://doi.org/10.1039/c8sc01035h.
[35] F. Conzuelo, A. Schulte, W. Schuhmann, Biological imaging with scanning electrochemical microscopy, Proc. R. Soc. A Math. Phys. Eng. Sci. 474 (2018), https://doi.org/10.1098/rspa.2018.0409.
[36] G. Wittstock, M. Burchardt, S.E. Pust, Y. Shen, C. Zhao, Scanning electrochemical microscopy for direct imaging of reaction rates, Angew. Chem. Int. Ed. 46 (2007) 1584–1617, https://doi.org/10.1002/anie.200602750.
[37] J. Petroniene, I. Morkvenaite-Vilkonciene, R. Miksiunas, D. Bironaite, A. Ramanaviciene, L. Mikoliunaite, A. Kisieliute, K. Rucinskas, V. Janusauskas, I. Plikusiene, S. Labeit, A. Ramanavicius, Evaluation of redox activity of human myocardium-derived mesenchymal stem cells by scanning electrochemical microscopy, Electroanalysis 32 (2020) 1337–1345, https://doi.org/10.1002/elan.201900723.
[38] J. Petroniene, I. Morkvenaite-Vilkonciene, R. Miksiunas, D. Bironaite, A. Ramanaviciene, K. Rucinskas, V. Janusauskas, A. Ramanavicius, Scanning electrochemical microscopy for the investigation of redox potential of human myocardium-derived mesenchymal stem cells grown at 2D and 3D conditions, Electrochim. Acta. 360 (2020), https://doi.org/10.1016/j.electacta.2020.136956.
[39] S. Rapino, R. Marcu, A. Bigi, A. Soldà, M. Marcaccio, F. Paolucci, P.G. Pelicci, M. Giorgio, Scanning electro-chemical microscopy reveals cancer cell redox state, Electrochim. Acta 179 (2015) 65–73, https://doi.org/10.1016/j.electacta.2015.04.053.
[40] G. Wittstock, T. Asmus, T. Wilhelm, Investigation of ion-bombarded conducting polymer films by scanning electrochemical microscopy (SECM), Fresenius J. Anal. Chem. 367 (2000) 346–351, https://doi.org/10.1007/s002160000389.
[41] C. Lefrou, R. Cornut, Analytical expressions for quantitative scanning electrochemical microscopy (SECM), ChemPhysChem 11 (2010) 547–556, https://doi.org/10.1002/cphc.200900600.
[42] R. Cornut, C. Lefrou, A unified new analytical approximation for negative feedback currents with a microdisk SECM tip, J. Electroanal. Chem. 608 (2007) 59–66, https://doi.org/10.1016/j.jelechem.2007.05.007.
[43] R. Cornut, S. Griveau, C. Lefrou, Accuracy study on fitting procedure of kinetics SECM feedback experiments, J. Electroanal. Chem. 650 (2010) 55–61, https://doi.org/10.1016/j.jelechem.2010.09.007.
[44] X. Zhao, P.M. Diakowski, Z. Ding, Deconvoluting topography and spatial physiological activity of live macrophage cells by scanning electrochemical microscopy in constant-distance mode, Anal. Chem. 82 (2010) 8371–8373, https://doi.org/10.1021/ac101524v.
[45] L. Biao, S.A. Rotenberg, M.V. Mirkin, Scanning electrochemical microscopy of living cells. 5. Imaging of fields of normal and metastatic human breast cells, Anal. Chem. 75 (2003) 4148–4154, https://doi.org/10.1021/ac0343127.
[46] C. Cai, B. Liu, M.V. Mirkin, H.A. Frank, J.F. Rusling, Scanning electrochemical microscopy of living cells. 3. Rhodobacter sphaeroides, Anal. Chem. 74 (2002) 114–119, https://doi.org/10.1021/ac010945e.